



NFκB mitigates the pathological effects of misfolded α1-antitrypsin by activating autophagy and an integrated program of proteostasis mechanisms

Amitava Mukherjee¹ · Tunda Hidvegi² · Patrick Araya¹ · Michael Ewing¹ · Donna B. Stolz¹ · David H. Perlmutter²

Received: 21 July 2017 / Revised: 1 May 2018 / Accepted: 2 May 2018 / Published online: 23 May 2018
© ADMC Associazione Differenziamento e Morte Cellulare 2018

Abstract

Intrahepatocytic accumulation of misfolded α1-antitrypsin Z variant (ATZ) is responsible for liver disease in some individuals with α1-antitrypsin deficiency (ATD), characterized by fibrosis/cirrhosis and predisposition to carcinogenesis. Previous results showing that accumulation of ATZ in model systems activates the NFκB signaling pathway have led us to hypothesize that downstream targets of NFκB are elements of a proteostasis response network for this type of proteinopathy. Here we show that only a subset of downstream targets within the NFκB transcriptomic repertoire are activated in model systems of this proteinopathy. Breeding of the PiZ mouse model of ATD to two different mouse models with NFκB deficiency led to greater intrahepatocytic accumulation of ATZ, more severe hepatic fibrosis, decreased autophagy and hyperproliferation of hepatocytes with massive ATZ inclusions. Specific downstream targets of NFκB could be implicated in each pathological effect. These results suggest a new role for NFκB signaling in which specific downstream targets of this pathway mediate an integrated program of proteostatic responses designed to mitigate the pathologic effects of proteinopathy, including autophagic disposal of misfolded protein, degradation of collagen and prevention of hyperproliferation.

Introduction

In the classical form of α1-antitrypsin deficiency (ATD) a point mutation leads to misfolding of the variant, α1-antitrypsin Z (ATZ), aberrant intracellular accumulation of the misfolded protein in liver cells and reduced levels of normally functioning α1-antitrypsin (AT) in the blood and body fluids [1]. Because, AT ordinarily functions as an inhibitor of neutrophil elastase and other neutrophil proteases, the loss of its function in ATD results in excessive proteolytic destruction of the pulmonary connective tissue matrix, manifest clinically as chronic obstructive pulmonary

disease (COPD). A sub-group of people with ATD develop chronic fibrotic liver disease and hepatocellular carcinoma. Because this hepatic pathology can be reproduced in animal models by transgenesis we know that it is caused by a gain-of-toxic function mechanism [1].

Although there is still relatively limited information about how ATD leads to liver fibrosis and cirrhosis, we know that accumulation of misfolded ATZ in liver cells activates downstream targets of TGFβ [2] and therein suspect that the TGFβ signaling pathway plays an important role. The mechanism of carcinogenesis is also undetermined. It is well known from pathological characterization of patients with liver disease due to ATD that only some of the hepatocytes contain globular inclusions reflecting massive accumulation of misfolded ATZ. There are always some hepatocytes that are devoid of the inclusions and these globule-devoid hepatocytes are also seen in the PiZ mouse mode of ATD [1]. Interestingly most of the hepatic carcinomas in ATD patients that have been described in the literature are characterized by absence of inclusions but are surrounded by cells bearing inclusions [3]. Using BrdU labeling in the PiZ mouse model of ATD, we found hyperproliferation of hepatocytes

Edited by: H.-U. Simon

✉ David H. Perlmutter
perlmutterd@wustl.edu

¹ Departments of Pediatrics and Cell Biology, University of Pittsburgh School of Medicine, Pittsburgh, PA, USA

² Department of Pediatrics, Washington University School of Medicine, St. Louis, MO, USA

in the resting state but almost all of the dividing hepatocytes were in the globule-devoid compartment [4]. This led to a hypothesis for the pathogenesis of carcinogenesis that envisions cross-talk between the two types of cells—signals emanating from replication-impaired, globule-containing hepatocytes chronically stimulate the proliferation and regeneration of globule-devoid hepatocytes [3]. This hypothesis was also supported by experiments in which normal hepatocytes were found to have a selective proliferative advantage in the liver when transplanted into PiZ mice [5].

To begin to determine how accumulation of misfolded ATZ leads to hepatic fibrosis and carcinoma, we investigated whether specific signaling pathways and cellular responses are activated when misfolded ATZ accumulates within cells. We used cell line models with inducible expression of ATZ and a mouse model with hepatocyte-inducible expression of ATZ (Z mouse model) because these systems would be ideal for detection of response pathways that were activated in relatively naive cells. The results showed that the autophagic response [6] and the NF κ B signaling pathways [7] are specifically activated. In subsequent studies, we have found that the autophagic response has an important role in the pathobiology of ATD [8, 9]. In terms of the NF κ B signaling, the results suggest that it has unique characteristics: it is activated independent of the UPR as there is relatively limited if any activation of the UPR when ATZ accumulates in cells [7]; it activates a relatively limited number of downstream targets [2] even though there is a marked increase in NF κ B-specific DNA-binding activity. One of the most notable changes in gene expression attributable to NF κ B signaling is marked downregulation of *Egr1* [2], a transcription factor which is essential for hepatocellular regeneration [10]. In this study, we began to investigate in further detail the effect of *Egr1* when NF κ B is activated by accumulation of misfolded ATZ in the liver. By breeding the PiZ mouse model of ATZ proteinopathy to two different models of NF κ B deficiency we were able to determine the impact of this particular NF κ B target and also discovered that several other targets of the NF κ B signaling pathway play a critical role in an integrated program of protective proteostasis mechanisms.

Results

Activation of NF κ B and downregulation of its downstream target, *Egr1*, in the PiZ mouse model of ATD

In previous studies using the Z mouse with hepatocyte-specific inducible expression of ATZ we found an

increase in NF κ B DNA-binding activity [7] but only a limited number of changes in expression of NF κ B targets were significant in a genome-wide transcriptomic profiling [2]. To initiate the current study, we used RT-PCR to investigate changes in expression of several known downstream targets of NF κ B in the liver of the Z mouse. In each case the level of expression of the genes in the liver of Z mice in the absence of doxycycline (ATZ expression induced) was compared to that in Z mice with doxycycline in the drinking water (ATZ expression off). The results showed marked downregulation of *Egr1* and confirmed that only a sub-group of the known downstream targets of NF κ B are activated (Fig. 1a), providing further evidence for the unique aspects of NF κ B activation in response to intracellular accumulation of misfolded ATZ.

Next, we investigated whether NF κ B is activated in another mouse model of ATD, the PiZ mouse. The PiZ mouse is a conventional transgenic mouse and so it differs from the Z mouse in having constitutive expression of ATZ [1]. Further the expression of ATZ is much higher and it is found in multiple cell types in addition to hepatocytes. It is also an ideal model of the ATD-liver disease with abundant globular inclusions, fibrosis and predilection for hepatocellular carcinoma [1]. To determine whether NF κ B is activated in the PiZ liver, electrophoretic mobility gel shift assays using the consensus NF κ B oligonucleotide showed marked increase in NF κ B DNA-binding activity in the PiZ liver (Fig. 1b). Next, using chromatin immunoprecipitation techniques (Fig. 1c), we found that antibodies to NF κ B p50, and to a lesser extent antibodies to p65, immunoprecipitate the *Egr1* promoter in PiZ liver but not in the liver of background strain C57/BL6. A non-specific IgG failed to immunoprecipitate the *Egr1* promoter in PiZ liver. We also investigated the expression of *Egr1* in PiZ liver by RT-PCR (Fig. 1d) and QPCR (Fig. 1e). There was a marked reduction in *Egr1* RNA in PiZ compared to C57/BL6 in each case. Together, these results indicate that PiZ liver is characterized by activation of NF κ B, binding of NF κ B to the promoter of a prototype NF κ B target, *Egr1*, and downregulation of *Egr1*.

Activation of NF κ B and downregulation of *Egr1* in the HTO/Z cell line model of ATD

To provide further validation of the NF κ B signaling pathway and *Egr1* as a downstream target of ATZ accumulation, we investigated the pathway in a cell line model of ATD, the HeLa-based HTO/Z cell line engineered for expression of ATZ that is regulated by doxycycline—i.e., expression of ATZ is induced when doxycycline is withdrawn. We also reasoned that this cell line model could be used for experimental perturbations that would complement what

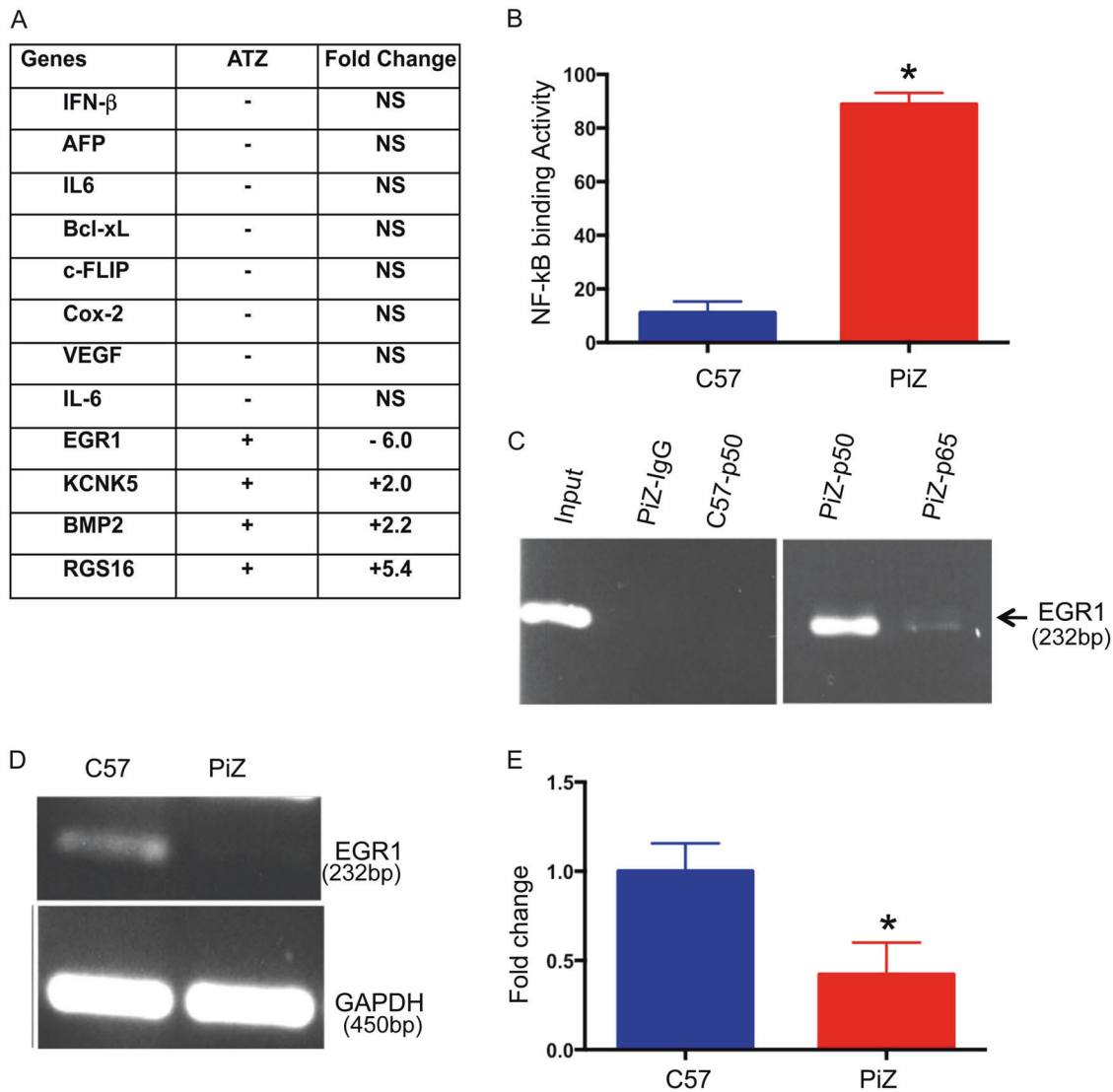


Fig. 1 Activation of NFκB and downregulation of Egr1 in the liver of the PiZ mouse model. **a** Transcriptional changes in the Z mouse model with liver-specific inducible expression of ATZ compared to known downstream targets of NFκB. In the left column genes that are known downstream targets of NFκB are listed and the arrow indicates whether the expression of each gene is increased or decreased by the action of NFκB in conventional inflammatory states. In the right column results of RT-PCR show whether these genes in gene expression occur in the liver of the Z mouse with liver-specific inducible expression [2] when ATZ expression is induced by withdrawal of doxycycline from the drinking water (+ indicates that the change in expression is reproduced in the Z mouse liver when ATZ gene expression is induced; - indicates that there is no change in expression of the gene when ATZ

gene expression is induced in the Z mouse). NS indicates no significant difference. **b** NFκB DNA-binding activity in PiZ and C57 (C57/BL6) mouse liver was assayed by electrophoretic mobility shift assay and the specific gel shift band was analyzed by densitometric scanning. Results are shown as mean ± SE for n = 3 mice each, p < 0.05. Asterisk indicates statistical significance from C57. **c** Chromatin immunoprecipitation assay in PiZ and C57 (C57/BL6) liver using antibodies to p50, p65, and non-specific IgG. **c** Expression of Egr1 in PiZ and C57 (C57/BL6) liver by RT-PCR. **d** Expression of Egr1 in PiZ and control (FVB/N) liver by QPCR. Results are shown as mean ± SE for n = 3 mice each, p < 0.01. Asterisk indicates statistical significance from control

can be determined in the mouse models. First, we investigated NFκB DNA-binding activity and found marked increases in the HTO/Z line when ATZ accumulation was induced by withdrawal of doxycycline as compared to the HTO/M line when wild-type AT had been induced (Fig. 2a). Second, we used immunoblot analysis and observed a marked decrease in steady-state levels of Egr1

when ATZ expression was induced in the HTO/Z cell line (Fig. 2b) and the decrease in Egr1 levels was also apparent when it was compared to the HTO/M cell line with expression of wild-type AT (Fig. 2c). These results indicate that ATZ accumulation activates NFκB and downregulation of Egr1 in one mammalian cell line model just as it does in the PiZ and Z mouse models.

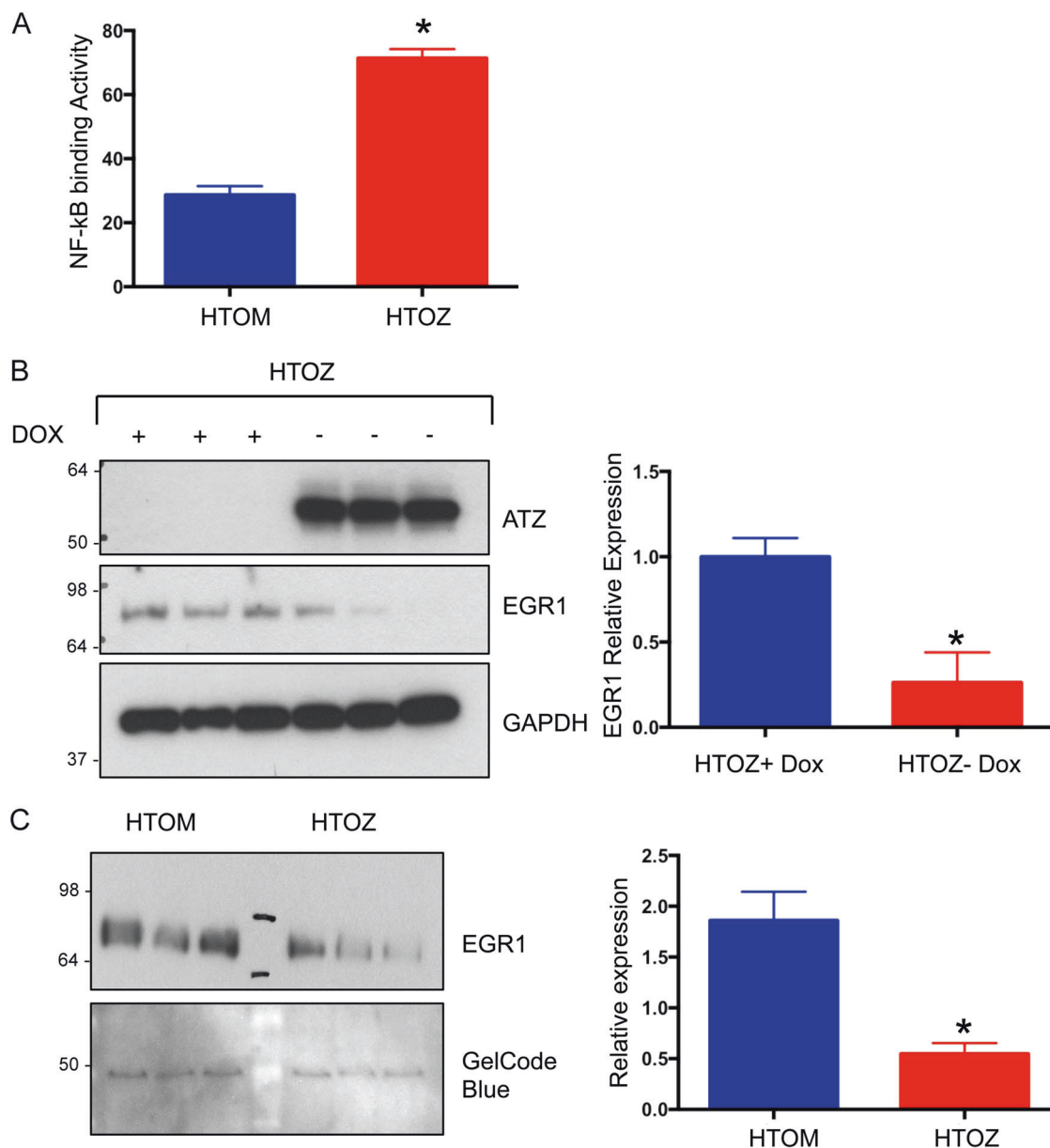


Fig. 2 Activation of NFκB and downregulation of Egr1 in the HTO/Z cell line model. **a** NFκB DNA-binding activity in HTO/Z and control HTO/M cell line was assayed by electrophoretic mobility shift assay and the specific gel shift band was analyzed by densitometric scanning. Results are shown as mean ± SE for $n = 3$ biological replicates each, $p < 0.01$. **b** Immunoblot analysis for steady-state levels of ATZ, Egr1, and GAPDH in the HTO/Z cell line in the presence or absence of

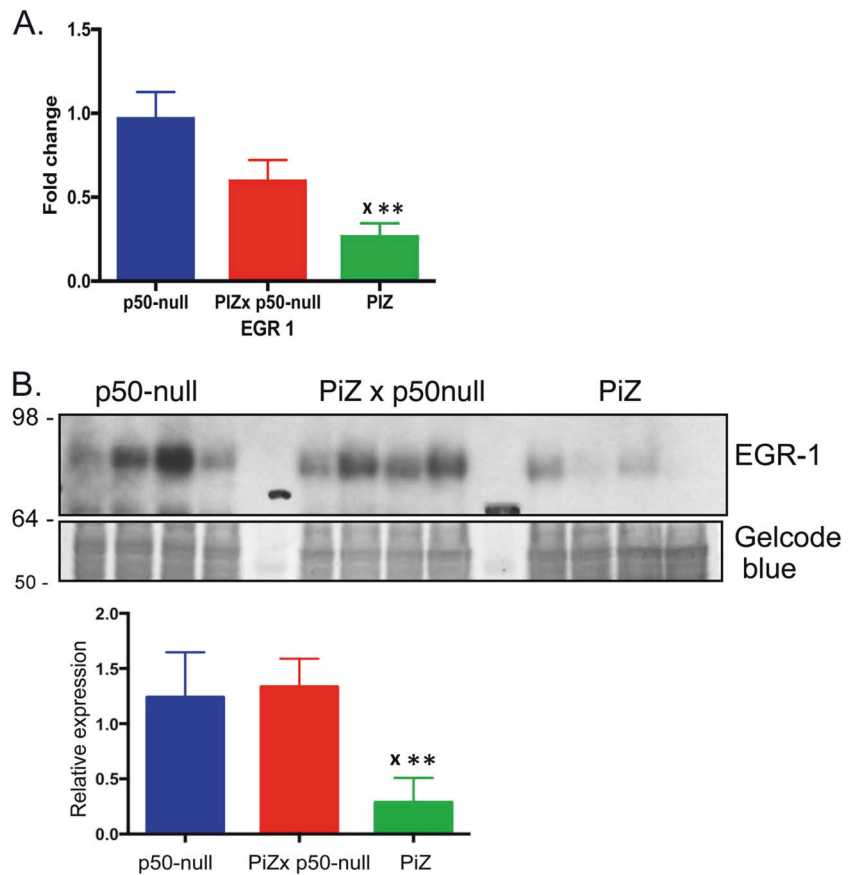
dox with relative densitometric intensity for Egr1 shown on the right in mean ± SE, $p < 0.05$. **c** Immunoblot analysis for steady-state levels of Egr1 in HTO/M and HTO/Z cell line in the absence of dox. Gelcode blue staining was used as a loading control. Results of densitometric scanning is shown at the right of **b** and **c** as mean ± SE, $p < 0.05$ for $n = 3$ biological replicates. Asterisk indicates statistical significance from control

Reversal of Egr1 downregulation in PiZ mouse by breeding to NFκB-deficient background

To determine the role of NFκB activation in hepatic pathological sequelae of ATZ accumulation we bred the PiZ mouse model to the NFκB p50-null mouse model [11]. The PiZ × p50-null offspring did not have any overall health phenotype. First we investigated Egr1 expression by QPCR (Fig. 3a). The results show that Egr1 downregulation is reversed in the

PiZ × p50-null compared to PiZ. Levels of Egr1 are significantly reduced in the PiZ mice compared to control. Levels of Egr1 are significantly increased in PiZ × p50-null mice compared to PiZ and not significantly different from control. Second, we determined steady-state levels of Egr1 in the liver by immunoblot analysis (Fig. 3b). The results show that hepatic Egr1 levels are similar in the PiZ × p50-null compared to p50-null; whereas, Egr1 levels are markedly decreased in the PiZ mice (Fig. 3b, lanes on the far right).

Fig. 3 Expression of Egr1 in PiZ × p50-null mouse liver. **a** QPCR. Results are shown as mean ± SE for $n = 3$ biological replicates each. Single asterisk indicates statistical significance for PiZ versus p50-null ($p < 0.01$) and double asterisk indicates statistical significance for PiZ × p50-null versus PiZ ($p < 0.05$). **b** Immunoblot analysis with densitometric scanning results at right. Gelcode blue staining is used as loading control. x indicates statistical significance for PiZ versus p50-null ($p < 0.01$) and double asterisk indicates statistical significance for PiZ versus PiZ × p50-null ($p < 0.01$) for $n = 4$ biological replicates



Effect of NFκB deficiency on hepatocyte proliferation in PiZ × p50-null mice

Next, we investigated the liver of the PiZ × p50-null mice for globular inclusions of misfolded ATZ (Fig. 4a). The results show a marked increase in number of globule-containing hepatocytes and the total area occupied by globules but not in the size of the globules in the PiZ × p50-null compared to PiZ mice, indicating that there are more cells with inclusions. Next, we used BrdU incorporation to determine the effect of NFκB deficiency on hepatocyte proliferation and, by double labeling for BrdU to identify dividing cells and for ATZ to identify globule-containing cells, we determined proliferation of globule-containing and globule-devoid hepatocytes (Fig. 4b). The results showed no difference in the overall BrdU incorporation in the PiZ × p50-null compared to the PiZ mice, indicating a similar hyperproliferative state for each. However, there was a striking increase in BrdU labeling of globule-containing hepatocytes in the PiZ × p50-null mice. These results indicate that hepatocytes that are most affected by accumulation of misfolded ATZ, as reflected by globular inclusions, are impaired in proliferation because of the actions of the NFκB pathway.

Effect of NFκB deficiency on fibrosis in PiZ × p50-null mice

Hepatic fibrosis is known to be a characteristic of the PiZ mice [1] and so here we sought to determine the role that NFκB signaling plays in that fibrotic condition. Sirius red staining showed a significant increase in the PiZ × p50-null compared to the PiZ mice and there was more nodular regeneration in the former group (Fig. 5a). These results provide evidence that NFκB signaling ordinarily mitigates the fibrotic effects of ATZ accumulation/proteotoxicity.

We also investigated expression of collagen and collagen-degrading genes in the livers of PiZ × p50-null mice as compared to PiZ and p50-null mice by QPCR (Fig. 5b). Although there were marked increases in collagen genes 1, 3, or 5 in PiZ mice compared to p50-null but there was no significant increase in any of these genes in the PiZ × p50-null compared to the PiZ mice (Fig. 5b). Expression of collagen 1, 3, and 5 was greater in the PiZ × p50-null than p50-null but only reached statistical significance for collagen 5 and acta 2. These results excluded the possibility that increased collagen expression was responsible for the increased fibrosis in PiZ × p50-null mice and so we next investigated expression of the collagen-

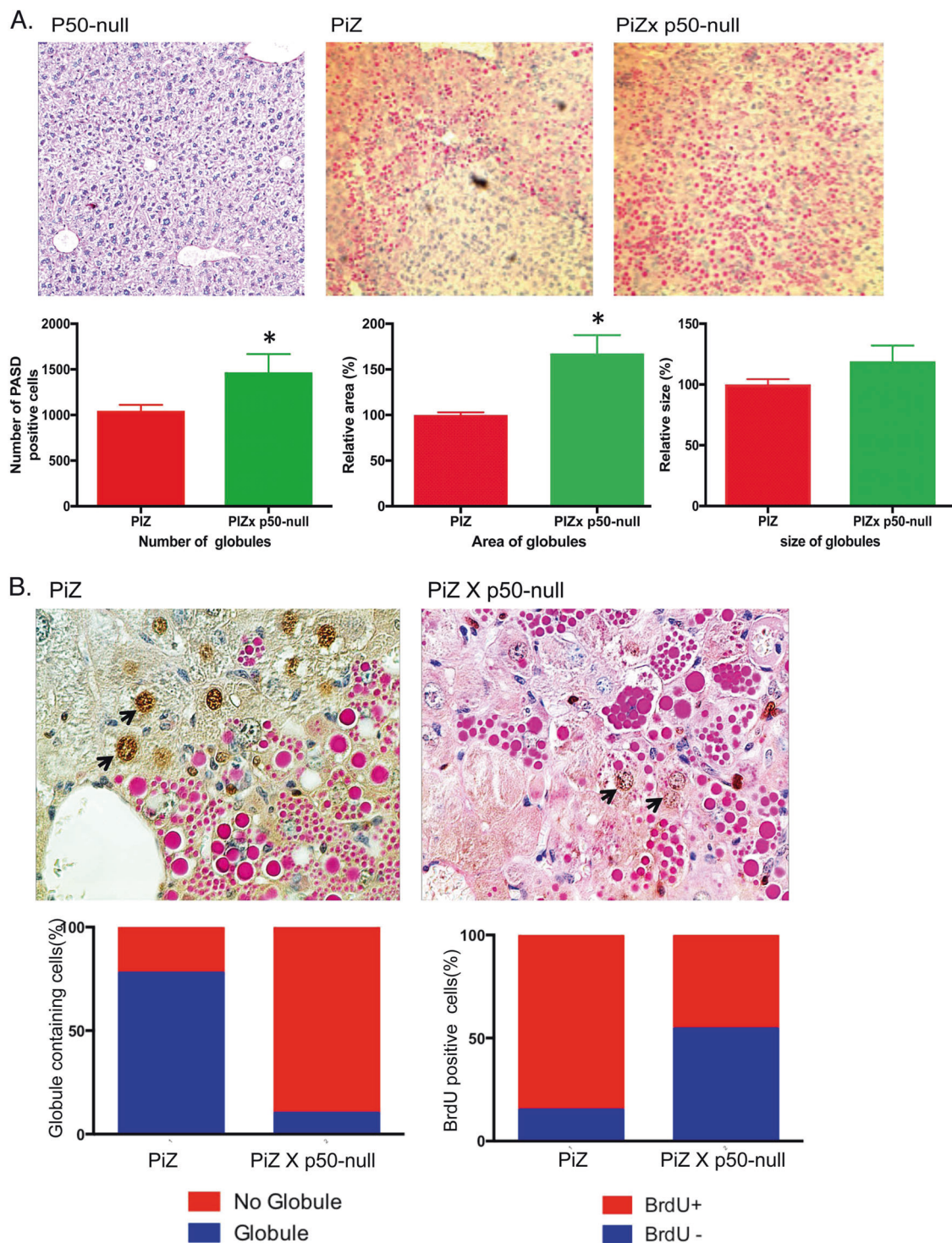
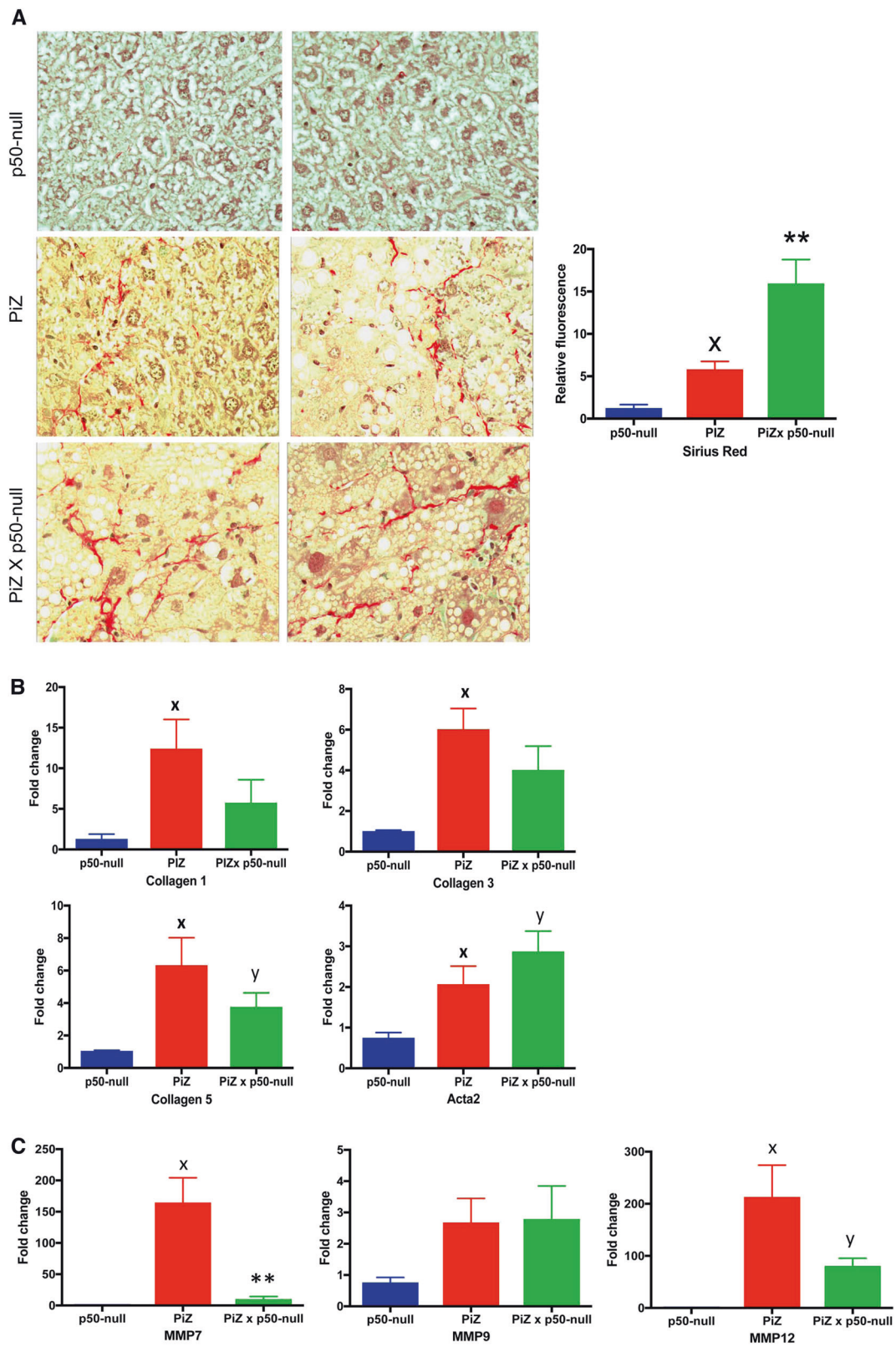


Fig. 4 Hepatic ATZ accumulation and hepatocyte proliferation in the PiZ × p50-null mouse compared to the PiZ mouse ($n = 3$ each). **a** PAS/D staining with quantitative morphometric analysis shown as mean ± SE for number of globules, area of globules and size of globules. Asterisk indicates statistical significance for PiZ ($p < 0.05$ for number

of globules and $p < 0.05$ for area of globules). **b** Double staining for PAS/D and BrdU with quantitative morphometry. The histogram on the left shows globule containing cells with BrdU+ in red and BrdU- in blue. The histogram on the right shows BrdU+ cells with globule containing cells in red and globule-devoid cells in blue

degrading metalloproteases (Fig. 5c). The results show increased MMP7 in the PiZ mice compared to p50-null and this increase was completely reversed in the PiZ × p50-null

mice. This pattern was similar for MMP12 but the reversal in the PiZ × p50-null mice did not reach statistical significance. Expression of MMP9 was increased in the PiZ



◀ **Fig. 5** Fibrotic response in PiZ × p50-null mouse liver compared to PiZ. **a** Sirius red staining with quantitative morphometry for p50-null, PiZ and PiZ × p50-null mice. On the left, examples of stained sections from two mice in each group is shown. On the right quantitative morphometry for $n = 3$ mice from each group is shown with x indicating statistical significance for PiZ vs p50-null and double asterisks indicating statistical significance for PiZ × p50-null vs PiZ ($p < 0.01$) **b** and **c**, expression by QPCR of collagen genes and collagen-degrading matrix metalloproteases, respectively ($n = 3$ each group). x indicates significant difference for PiZ compared to p50-null; double asterisks indicate significant difference for PiZ × p50-null compared to PiZ; y indicates significance for PiZ × p50-null compared to p50-null

and PiZ × p50-null but it was not a statistically significant increase and there was no difference between PiZ and PiZ × p50-null. The *MMP7*, *MMP9*, and *MMP12* genes are known to have NFκB consensus elements in their upstream regulatory regions. These results suggest that collagen accumulation in the liver of the PiZ × p50-null mice is due to decreased expression of collagen-degrading matrix metalloprotease, specifically MMP7 and possibly MMP12, and imply that the transcriptional effects of NFκB signaling are designed to counteract collagen deposition and fibrosis by selectively activating this metalloprotease.

To exclude the possibility that these results are for some reason peculiar to the p50-null mouse model, we also bred the PiZ mice to mice with liver-specific deletion of IκB kinase β (*IKKβΔhep*), a model that is deficient in NFκB signaling by a completely different mechanism [12]. In the PiZ × *IKKβΔhep*, we also found increased number of globule-containing hepatocytes (Fig. 6a) and quantitative measurement of hepatic hydroxyproline showed a marked increase in collagen deposition as compared to the PiZ mice (Fig. 6b). In terms of expression of collagen and metalloprotease genes, downregulation of the matrix metalloproteases is the common thread between the PiZ × *IKKβΔhep* and PiZ × p50-null mice. In Fig. 6c there is a profound decrease in MMP7 and MMP9 in the PiZ × *IKKβΔhep* as compared to the PiZ mice. A similar pattern is seen for MMP12 but the decrease in the PiZ × *IKKβΔhep* did not reach statistical significance. These results suggest that regulation of collagen degradation is the mechanism by which NFκB signaling affects fibrogenesis in this model just as it does in the completely different PiZ × p50-null model. The changes in matrix metalloprotease gene expression in the PiZ × *IKKβΔhep* model are also likely to be particularly important because there is a paradoxical decrease in collagen gene expression, specifically collagens 1 and 5, in the PiZ × *IKKβΔhep* as compared to the PiZ mice. Taken together, these results indicate that collagen deposition is more severe when the NFκB pathway is impaired and imply that NFκB signaling is a form of proteostasis regulation that mitigates hepatic fibrosis in ATD by increasing transcription of collagen-degrading enzymes.

Effect of NFκB deficiency on autophagy in mouse and cell line models of ATD

Next, we investigated the possibility that NFκB activation affects autophagy in the liver in ATD. First, we investigated the liver of the PiZ × p50-null mice for measures of autophagy. Each of the mice had been bred onto the GFP-LC3 background and thus we could monitor for GFP+ autophagosomes in the liver (Fig. 7a). The results show the presence of GFP+ vesicles in the liver of normally fed PiZ mice. It is well known that GFP+ autophagosomes are only seen in the liver of GFP-LC3 mice after starvation (6) and so the presence of GFP+ vesicles in normally fed PiZ mice indicate that autophagy has been activated by ATZ accumulation, consistent with our previous results using the Z mouse model with hepatocyte-specific inducible expression of ATZ [6]. Interestingly, here we found a marked and statistically significant decline in the liver of PiZ × p50-null mice compared to the PiZ mice (Fig. 7a). Next we examined liver for LC3 isoforms (Fig. 7b) and the results show a marked and statistically significant increase in the LC3-II to LC3-I ratio in the PiZ compared to p50-null mice and this is completely reversed in the PiZ × p50-null mice. These results suggest that autophagy is decreased when NFκB signaling is deficient and therefore that NFκB signaling plays a role in the activation of autophagy that is elicited by intracellular ATZ accumulation.

We also investigated the expression of several autophagy genes in the liver of PiZ × p50-null mice compared to PiZ and p50-null mice using qRT-PCR (Fig. 7c). The results show that changes in expression of core autophagy genes p62, beclin 1, ATG5, ATG7, and ATG12 at the RNA level are not the basis for increased autophagy in the PiZ mice compared to controls nor for the decrease in autophagy in the PiZ × p50-null compared to the PiZ mice, thereby suggesting that post-transcriptional, translational, post-translational, or functional changes in these genes or changes in expression of other autophagy genes are responsible for overall autophagy function shown in previous studies (6,8) and in Fig. 7a, b. More specifically, in Fig. 7c, there were no significant differences in the PiZ × p50-null compared to the PiZ mice for p62, ATG7, and ATG12. For beclin 1 there was a significant decrease in the PiZ compared to the p50-null and this was significantly reversed in the PiZ × p50-null mice. For ATG5 there was a similar pattern but the levels in the PiZ × p50-null were not significantly different than PiZ or p50-null. We do not know the explanation for decreased levels of beclin 1 and ATG5 RNA in the liver of the PiZ mouse as compared to the p50-null. Decreased levels of beclin 1 and ATG5 RNA could possibly reflect the chronic proteotoxic state of the PiZ mouse liver. Although there is limited information about what happens to RNA levels of autophagy genes in

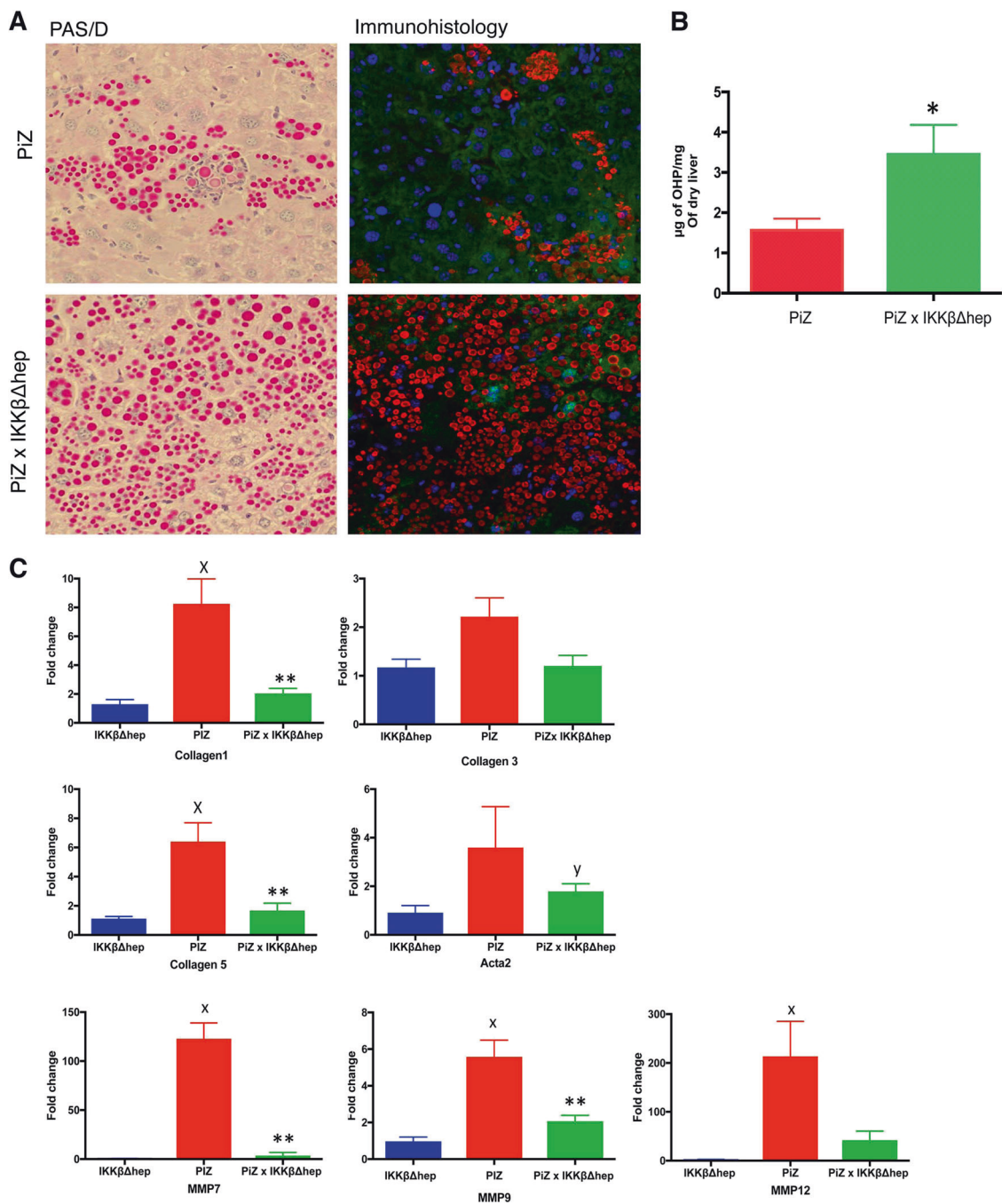


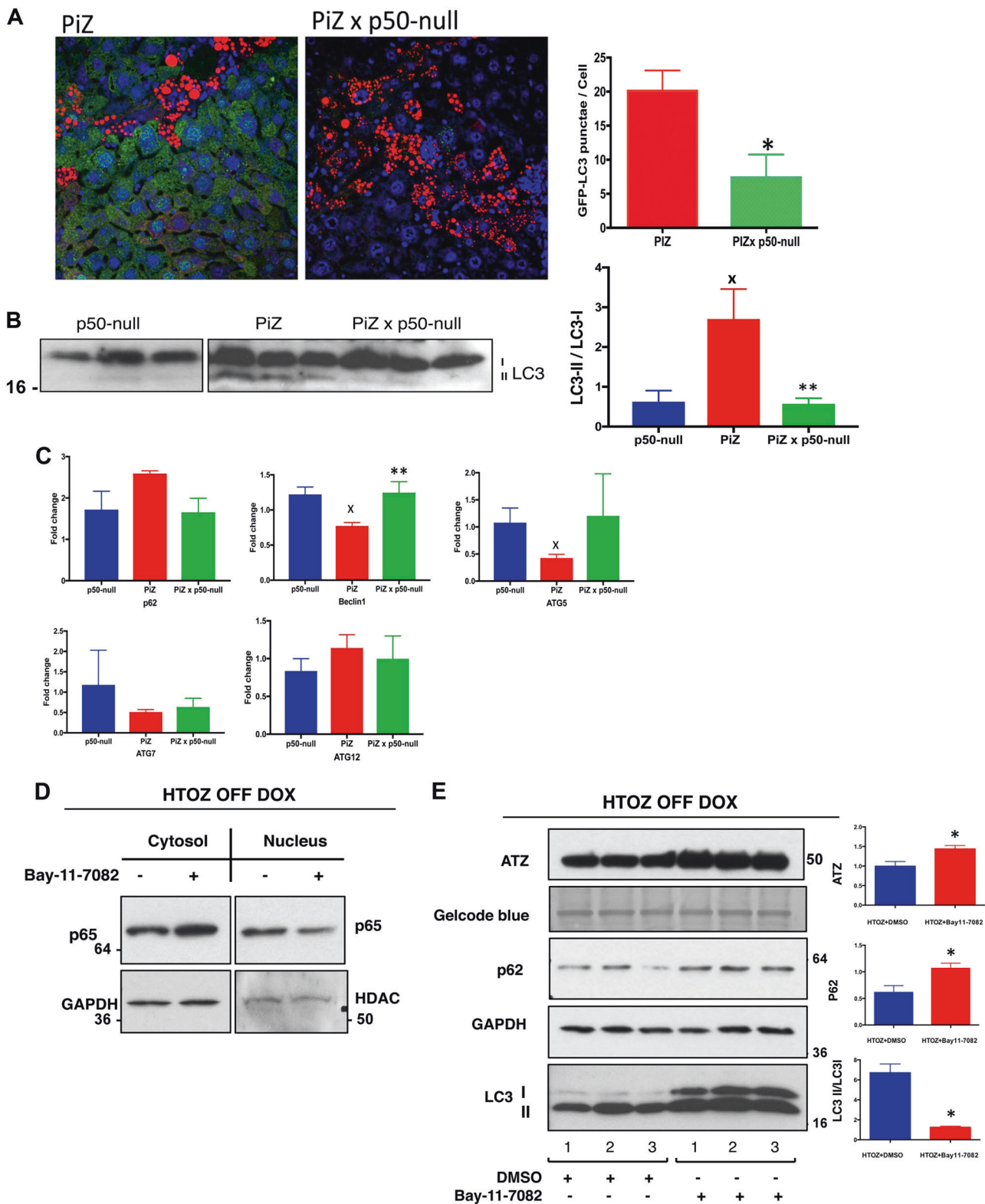
Fig. 6 Hepatic ATZ accumulation and fibrotic response in PiZ × IKKβΔhep mouse compared to PiZ mouse. **a** Staining of liver sections with PAS/D (left) and anti-AT antibody (Immunohistology—right); **b** Hepatic hydroxyproline content, $n = 3$ for each group. Asterisk indicates statistical significance ($p < 0.05$); **c** Expression of collagen and

collagen-degrading metalloproteases by QPCR, $n = 3$ for each group. *x* indicates significant difference for PiZ compared to IKKβΔhep; double asterisk indicates significant difference for PiZ × IKKβΔhep compared to PiZ; *y* indicates significant difference for PiZ × IKKβΔhep compared to IKKβΔhep

chronic proteotoxic states, beclin 1 RNA levels are decreased in the brain in huntington disease [13] and Alzheimer disease [14].

We also investigated the effect of inhibiting NFκB signaling on autophagy in the HTO/Z cell line model by incubating the cells for 18 h with 10 μM BAY 11-7082

(Fig. 7d, e). First, this perturbation was shown to inhibit NFκB as reflected by a reversal in the amount of NFκB p65 in the cytosol as compared to the nucleus. Next, we found that BAY 11-7082 mediated marked decreases in the LC3-II to LC3-I ratio and a significant increase in the levels of p62, consistent with a decrease in autophagic



activity. Furthermore, the effect of BAY 11-7082 leads to increased levels of ATZ accumulation. Thus, these results are also consistent with the concept that one of the consequences of intracellular ATZ accumulation is activation

of the NF κ B signaling pathway, and this pathway plays a role in induction of autophagy and enhanced degradation of the misfolded protein as a unique proteostasis mechanism.

◀ **Fig. 7** Effect of NFκB deficiency on hepatic autophagic response in PiZ × p50-null mice and of NFκB inhibition in the HTO/Z cell line model. **a** Immunostaining of GFP+ autophagosomes. Quantification of GFP-LC3 puncta per cell is shown as mean ± SE for $n = 3$ each. Asterisk indicates statistical significance ($p < 0.05$). **b** Immunoblot analysis for LC3 isoforms in the liver of the p50-null, PiZ and PiZ × p50-null mice with relative densitometric analysis. x indicates statistical significance for PiZ compared to p50-null and double asterisk indicates statistical significance for PiZ × p50-null compared to PiZ ($p < 0.05$); **c** Expression of autophagy genes in the liver of the PiZ × p50-null vs PiZ and vs p50-null mice using qRT-PCR is shown as fold-change (mean ± SE for $n = 3$ each). x indicates statistical significance for PiZ vs p50-null and double asterisks indicate statistical significance for PiZ × p50-null compared to PiZ. **d** Effect of Bay 11-7082 on NFκB p65, ATZ, p62, and LC3 isoform levels in HTO/Z cell line. Asterisk indicates statistical significance ($p < 0.05$ for p62 and $p < 0.01$ for LC3-II to LC3-I ratio)

Expression of NFκB target genes in liver from patients with ATD

Finally, we used qRT-PCR to investigate the expression of Egr1, MMP7, and MMP12 in the liver of patients with ATD as compared to normal liver (Fig. 8). Native liver tissue collected at the time of liver transplantation from 5 patients with ATD and end-stage liver disease was compared to 'normal' liver tissue from victims of fatal accidents collected prior to withdrawal of life support. The results showed a statistically significant increase in MMP7. MMP12 expression was also increased but this difference did not reach statistical significance ($p = 0.07$). Egr1 expression did not show a significant decline but we cannot exclude the possibility that this difference in human tissues compared to the PiZ mouse model is due to the secondary effects of end-stage liver disease on the human liver samples.

Discussion

The classical form of ATD is a proteinopathy characterized by accumulation of misfolded ATZ in early compartments of the secretory pathway. The primary pathological consequences are fibrosis/cirrhosis and carcinoma in the liver, presumably affecting this organ because it is a site of abundant synthesis of this secretory protein. One of the most intriguing aspects of the way this disease manifests itself clinically is that many homozygotes completely escape liver disease or experience minimal clinical sequelae. This has led us to hypothesize that genetic and/or environmental modifiers can protect some homozygotes and, furthermore, that these modifiers act through proteostasis mechanisms, such as pathways for degradation of the misfolded variant or signaling pathways that allow the affected cells to adapt to proteotoxicity [1, 9]. To pursue this hypothesis, we have used systems with inducible

expression of ATZ to characterize the relevant degradative and adaptive signaling pathways. In this study, we investigated the consequences of NFκB activation that is elicited when ATZ accumulates using inducible systems. First, we found that the repertoire of downstream targets of NFκB activated in several cell line and mouse model systems is relatively limited compared with the targets that characterize the NFκB response to classical inducers, such as cytokines. The transcription factor Egr1, which plays a role in hepatic regeneration [10], is one of the downstream targets of NFκB in the setting of intracellular ATZ accumulation and, interestingly, this response is characterized by marked downregulation of Egr1. Second, we found that hepatic ATZ accumulation and hepatic fibrosis were worse in the PiZ mouse model of ATD bred to two different models that are deficient in NFκB signaling, indicating that NFκB activation is ordinarily acting to prevent fibrosis. In the absence of NFκB signaling autophagy was inhibited and thus an effect on autophagy could represent how NFκB activation plays a role in the hepatic fibrotic response. Expression of collagen-degrading matrix metalloproteases that are targets of NFκB were also depressed in the absence of NFκB signaling. Furthermore, downregulation of Egr1 was reversed and this was accompanied by increased proliferation of hepatocytes with massive ATZ inclusions, suggesting that Egr1 downregulation in response to NFκB plays a role in the hyperproliferative state that characterizes the liver in the PiZ mouse model. Taken together, these results suggest three very specific ways that NFκB signaling influences the hepatic pathology of ATD.

Several aspects of how NFκB is activated in response to intracellular ATZ accumulation, as described here, suggest that it is a distinct form of the NFκB signaling pathway. First, previous studies have shown that it is not a part of the unfolded protein response because there is minimal, if any, UPR signaling elicited under conditions in which ATZ expression is induced [2]. Second, the repertoire of NFκB downstream targets is limited compared to what is seen when the pathway is activated by cytokines or tunicamycin [15, 16]. This could mean that there is something unique about the composition of the NFκB multiprotein complex that assembles and affects binding/activation of downstream target genes or that other signaling responses elicited by ATZ accumulation affect the NFκB-dependent transcriptional repertoire. These possibilities will be important to investigate in future studies.

One of the most important findings in this study is inhibition of autophagy when ATZ accumulates in the absence of NFκB signaling. This was observed in both the PiZ × p50-null and PiZ × IKKβ^Δhep models and therefore could not be attributable to the NFκB-independent mechanism for induction of autophagy that has been linked to IKKβ [17]. Furthermore, we found that autophagy

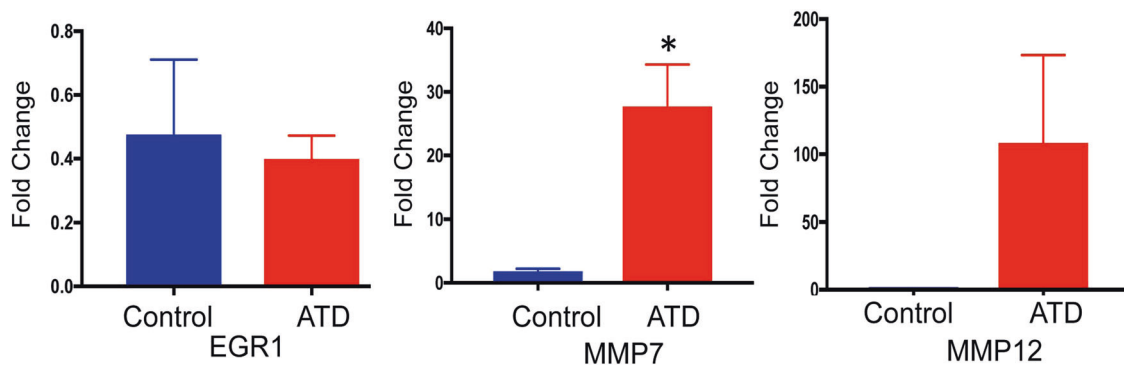


Fig. 8 Expression of NF κ B target genes Egr1, MMP7, and MMP12 in livers from ATD patients ($n = 5$) and normal controls ($n = 7$) by qRT-

PCR. Results are shown as fold change (mean \pm SE). Asterisk indicates statistically significant difference

was inhibited in a cell line model when NF κ B signaling was dampened pharmacologically. We know that autophagy is specifically activated by intracellular accumulation of ATZ and that it plays a critical role in degradation of ATZ [6, 8, 9]. This makes it highly likely that inhibition of autophagy is at least partially involved in the increased hepatic ATZ load and proteotoxicity in the PiZ \times p50-null and PiZ \times IKK β Δ hep mouse models. Further, these results implicate the stimulation of autophagy as one of the mechanisms by which the NF κ B signaling pathway is designed to prevent fibrosis in the ATZ proteinopathy. In a previous study, we found that RGS16 is upregulated when ATZ accumulates in the liver and speculated that it might play a role in activating autophagy because hepatic autophagy is induced when hepatic G $_{13}$ is deleted [18]. Interestingly, there is a consensus element for NF κ B in the upstream flanking region of RGS16 and NF κ B is known to upregulate RGS16 [19]. Thus, it is possible that the effect of NF κ B activation on autophagy is mediated, to at least some extent, by RGS16 upregulation.

Our results also suggest that the NF κ B response plays an important role in hepatocyte proliferation in the PiZ mouse model of ATD. BrdU labeling studies have shown that hepatocytes with massive accumulation of ATZ, globule-containing hepatocytes, are impaired in proliferation. The results of this study suggest that this is mediated by NF κ B-mediated downregulation of Egr1 because replication of globule-containing hepatocytes was increased in the PiZ \times p50-null mouse model. Although this action of NF κ B could be viewed as protective by slowing down the cells which are damaged, we have found that these cells are indirectly responsible for hyperproliferation of globule-devoid cells with lesser accumulation of ATZ [3, 4] and for transplanted normal hepatocytes [5] by setting up a selective proliferative advantage for less damaged, or undamaged, cells. This concept is consistent with the idea that NF κ B signaling is designed for acute and short-term cellular proteostasis and, in doing so, prevents ATZ accumulation and hepatic

fibrosis but when activated chronically it could indirectly and, paradoxically, promote carcinogenesis.

Taken together, these results provide evidence that the NF κ B signaling pathway can uniquely activate a limited repertoire of downstream targets to protect an affected organ from proteinopathy. This type of NF κ B signaling is particularly interesting because it appears to be designed to counteract several different damaging aspects of the proteinopathy including accumulation of the misfolded protein, collagen deposition, and hyperproliferation. Although NF κ B signaling pathway is well known for its role in the inflammatory response and has recently been implicated in limiting tissue damage from inflammatory states [20], this report provides some initial evidence that it plays a regulatory role in the pathological signature of cellular protein overload.

Experimental procedures

Materials

Rabbit anti-human AT antibody was purchased from the DAKO (Santa Barbara, CA) and goat anti-human AT from Diasorin (Stillwater, MN). Antibody to GAPDH and LC3 were purchased from Sigma-Aldrich (St. Louis, MO) and antibodies to p62 and EGR1 were purchased from cell Signaling Technology Inc (Danvers, MA). Doxycycline was purchased from Sigma and prepared 1 mg/ml in water. NF- κ B inhibitor BAY 11-7082 was purchased from Santacruz (stock solution 100 mM made in DMSO).

Cell lines

The human epidermal HeLa cell line with doxycycline-regulated expression of ATZ (HTO/Z) has been described [7]. HTO/M is a HeLa cell lines with doxycycline-regulated expression of wild-type AT [7]. The inducible cell lines

were cultured in the absence of doxycycline for at least 2 weeks to induce expression of AT. The cells were then subcultured into separate monolayers, incubated for 48 h in fresh complete growth medium and then for 18 h in the absence or presence of Bay 11 (10 μM). The cell homogenates (20 μg) were analyzed by immunoblot for AT, p62, LC3, and GAPDH. At least three separate experiments were done in each case.

Transgenic mice

PiZ mice bred onto the C57/BL6 background have been described previously [5] and then mated to the GFP-LC3 [6] so that autophagy could be monitored in all of the experiments. The transgene that was used to generate the PiZ mouse is a genomic fragment of DNA that contains the coding regions of the ATZ gene together with introns and ~2 kilobases of upstream and downstream flanking regions [21]. Z mice, with liver-specific inducible expression of ATZ have been previously described [2]. The p50-null mice, originally generated by Sha et al. [11] were purchased from the Jackson Laboratories repository 6097 and then bred to PiZ mice. Mice with deletion for IKKβ specifically in liver hepatocytes (IKKβΔhep) were kindly provided by Dr. Michael Karin (University of California, San Diego). They were generated with a conditional and nearly complete IKKβ loss-in-hepatocytes [12]. These mice were then bred to PiZ mice. In each of the experiments p50-null or IKKβΔhep mice were used as the negative control. Sections of liver tissue were stained with hematoxylin and eosin, PAS, PAS after diastase treatment, BrdU, Sirius Red using standard techniques [2, 22, 23]. The number of AT-containing globules was quantified blindly by counting cells in 6 microscopic fields of 10 different sections for each liver. Sirius Red staining was also quantified by blindly analyzing 6 microscopic fields of 10 different sections for each liver using percent area stained red as determined by ImageJ software [8]. For the incorporation of BrdU in liver subcutaneous implantation of BrdU-filled osmotic pumps designed for sustained release (Alzet 2001; flow rate 20 μg/h) was performed. The frequency of BrdU labeled nuclei were determined by imaging at least three random fields, magnification ×400 and at least 300 cells and nuclei in each tissue section were counted [4].

Sections of liver tissue were also doubly stained with anti-GFP together with anti-AT to detect GFP+ autophagosomes and their relationship to ATZ accumulation exactly as described previously [6]. At least six images from the livers of three mice were analyzed. Each image was split into three monochromatic channels, green for GFP-LC3, red for ATZ and blue for nuclei. The blue and green channels were used for quantification and adjusted to a threshold that would exclude background GFP from the staining of puncta

by GFP. The number of GFP puncta and the number of nuclei were counted using ImageJ analyze partner option. The number of puncta divided by the number of nuclei in the field provided the number of puncta/cell. All animal studies were approved by the IACUC of the University of Pittsburgh.

Western blot

For immunoblot analysis to detect AT, p62, EGR1, GAPDH, or LC3, cells were lysed in 50 mM Tris-HCl (pH 8.0), 150 mM NaCl, 1% NP-40. Protein levels were quantified using the BCA protein assay (Pierce Biotechnology, Rockford, IL). A total of 10–50 μg samples were loaded onto precast gels. PVDF membranes were blocked in 5% milk in TBS with 0.1% Tween 20 (TBST) and then incubated with primary antibody in 5% milk TBST solution. Horse radish peroxidase anti-goat, anti-rabbit, or anti-mouse IgG (Jackson Labs, Bar Harbor, ME) were used as secondary antibodies in TBST. Blots were visualized with Super Signal West Dura or West Femto from Pierce. For immunoblots on liver, the liver was snap frozen in liquid nitrogen and stored at –80 °C. Liver was homogenized in 50 mM Tris-HCl, pH 8.0, 150 mM NaCl, 2 mM KCl, 2 mM MgCl₂, 0.5% Triton X-100, 0.5% deoxycholic acid containing 0.1 mM phenylmethylsulfonic acid and complete protease inhibitor cocktail from Roche. Total protein concentration was measured by BCA assay (Pierce). Soluble and insoluble fractions were separated by centrifugation (14,000 r.p.m., 10 min, 4 °C). The insoluble pellet was washed twice in 50 mM Tris-HCl (pH 7.4, 150 mM NaCl) and resuspended in 50 mM Tris-HCl (pH 6.8, 5% SDS, 10% glycerol). Equal amounts of total protein (1 μg) were loaded on 10% SDS-PAGE gels. After transfer to PVDF membrane, the blots were blocked in TBST containing 5% non-fat milk for 1 h at RT, then goat-anti-human AT antiserum (Diasorin, 1:2500) was applied followed by three washes. Donkey anti-goat IgG-HRP (Santa Cruz, 1:1,000,000) and West Dura (Pierce) was used for detection of AT. The blots were stripped (Pierce) and after the blocking step anti-mouse GAPDH (US Biologicals, 1:10,000) and rabbit anti-mouse IgG-HRP (Jackson Labs, 1:5000) were used to detect GAPDH.

Chromatin immunoprecipitation (ChIP) assay

ChIP was performed using a commercially available ChIP Assay Kit, Millipore according to manufacturer's instructions. Liver tissues from PiZ and control mice were processed and DNA-bound proteins were immunoprecipitated using anti-p50 and p65 antibodies. Mouse IgG was used as negative control (Santa-Cruz Biotechnology). The coprecipitated DNA, samples were then subjected to

amplification by employing primers (For: 5'-CTTA-TATGGAGTGGCCCAATATGG-3'; and Rev: 5'-TTCA CGTCACTCCGGGTCCT-3'), which amplified the promoter region (209 bp) of EGR1. Unprecipitated chromatin was used as input material.

RNA isolation and RT-PCR

Total RNA was isolated from powdered liver tissues according to the protocol supplied with TRIZOLi Reagent (Invitrogen, Life Technologies). The concentration of the RNA samples were determined using a NanoDrop spectrophotometer and cDNAs were made from RNA (2 µg) using high-capacity RNA-to-cDNA™ Kit (Thermo Fisher Scientific) following manufacturer's instructions. EGR1 PCR was done using Primers (For: 5'-TCGGCTCCTTCTCACTCA-3'; and Rev: 5'-CTCATAGGGTTGTTGCTCGG-3') along with GAPDH (For: 5'-ACCACAGTCCATGCCATCAC-3' and Rev: 5'-CACCACCCTGTTGCTGTAGCC-3') for loading control.

Real-time PCR

Quantitative reverse transcription-PCR (qRT-PCR) was performed under universal cycling variables on an ABI 7300HT instrument using commercially available target probes and Master mix (all from Applied Biosystems). Detection of human ATZ, mouse EGR1, Collagens (1, 3, and 5), Acta 2, MMPs (7, 9, and 12), p62, ATG5, ATG7, ATG12, Beclin 1, and human EGR1, MMPs (7 and 12) were achieved using specific Taqman Gene Expression Assays (Hs01097800_m1, Mm00656724_m1, Mm00801666_m1, Mm00802331_m1, Mm00483675_m1, Mm00487724_m1, Mm00442991_m1, Mm00500554_m1, Mm01187303_m1, Mm01187303_m1, Mm00512209_m1, Mm00503201_m1, Mm01265461_m1, Hs00152928_m1, and Hs01042796_m1, Hs00159178_m1, respectively). Real time reactions were run using the following cycling parameters: 95 °C for 12 min, followed by 40 cycles of 95 °C for 15 s and 60 °C for 1 min. Differential gene expression was calculated by the $\Delta\Delta CT$ calculation [24].

Electrophoretic mobility shift assay (EMSA)

Experiments were performed using the LightShift Chemiluminescent EMSA Kit (Pierce) according to the manufacturer's protocols. Each 20 µL binding reaction contained 1× binding buffer (10 mM Tris, 50 mM KCl, 1 mM DTT), 2.5% glycerol and 10 mM KCl 20 fmol DNA probe was used and 0.5 µg protein. The binding reactions were allowed to incubate at room temperature for 1 h. A precast 6% polyacrylamide DNA retardation gel (Invitrogen) was pre-run for 60 min at 100 V, and then 5 µL of 5× loading buffer

was added to the binding reaction, and subsequently 20 µL of the reaction was run on the gel at 100 V for 45 min. The gel was then transferred to a positively charged modified nylon membrane (Ambion) for 30 min at 100 V, and subsequently UV-crosslinked to the membrane at 120 µJ/cm². The membrane was then incubated with buffers (LightShift Blocking Buffer with stabilized Streptavidin-Horse Radish Peroxidase conjugate, Wash Buffer, Substrate Equilibration Buffer, Luminol/Enhancer Solution and Peroxide Solution) according to manufacturer's protocol, then exposed to film and developed.

Statistical analysis

Student's *t*-test was used for most comparisons but the Welch modified *t*-test was used to compare experimental groups that were not paired and did not assume equal variances. The graphs were made using the Prism software application. All fluorograms were subjected to densitometry. The data are shown as mean ± SE.

Acknowledgements The authors are indebted to Kelly Michel, Houming Cai and Pamela Hale for technical assistance. The studies were supported by the NIH grants DK096990 and DK100289 and by endowment funds from the Childrens Hospital of Pittsburgh of UPMC.

Author contributions Conceptualization: A.M. and D.H.P.; Methodology: A.M., D.B.S., T.H., and D.H.P.; Investigation: A.M., T.H., M. E., D.B.S., and P.A.; Writing—original draft: A.M. and D.H.P.; Writing—review and editing: A.M. and D.H.P.; Funding acquisition, D.H.P.; Resources, D.H.P.; Supervision, T.H. and D.H.P.

Compliance with ethical standards

Conflict of interest The authors declare no conflicts of interest.

References

- Ghose R, Chu A, Wang Y, Perlmutter DH. Mysteries of $\alpha 1$ -antitrypsin deficiency: emerging therapeutic strategies for a challenging disease. *Dis Model Mech*. 2014;4:411–9.
- Hidvegi T, Mirmics K, Hale P, Ewing M, Beckett C, Perlmutter DH. Regulator of G signaling 16 is a marker for the distinct ER stress state associated with aggregated mutant $\alpha 1$ -antitrypsin Z in the classical form of $\alpha 1$ -antitrypsin deficiency. *J Biol Chem*. 2007;282:27769–80.
- Rudnick DA, Perlmutter DH. Alpha-1-antitrypsin deficiency: a new paradigm for hepatocellular carcinoma in genetic liver disease. *Hepatology*. 2005;42:514–21.
- Rudnick DA, Liou Y, An J-K, Muglia LJ, Perlmutter DH, Teckman H. Analyses of hepatocellular proliferation in a mouse model of alpha-1-antitrypsin deficiency. *Hepatology*. 2004;39:1048–55.
- Ding J, Yannam GR, Roy-Chowdhury N, Hidvegi T, Basma H, Rennard SI, et al. Spontaneous hepatic repopulation in transgenic mice expressing mutant human $\alpha 1$ -antitrypsin by wild-type donor hepatocytes. *J Clin Invest*. 2011;121:1930–4.
- Kamimoto T, Shoji S, Hidvegi T, Mizushima N, Umebayashi K, Perlmutter DH, et al. Intracellular inclusions containing mutant

- α 1-antitrypsin Z are propagated in the absence of autophagic activity. *J Biol Chem.* 2006;281:4467–76.
7. Hidvegi T, Schmidt BZ, Hale P, Perlmutter DH. Accumulation of mutant α 1ATZ in the ER activates caspases-4 and -12, NF κ B and BAP 31 but not the unfolded protein response. *J Biol Chem.* 2005;280:39002–15.
 8. Hidvegi T, Ewing M, Hale P, Dippold C, Beckett C, Kemp C, et al. An autophagy-enhancing drug promotes degradation of mutant α -antitrypsin Z and reduces hepatic fibrosis. *Science.* 2010;329:229–32.
 9. Perlmutter DH. Alpha-1-antitrypsin deficiency: Importance of proteasomal and autophagic degradative pathways in disposal of liver disease-associated protein aggregates. *Annu Rev Med.* 2010;62:333–45.
 10. Liao Y, Shikapwashya ON, Shteyer E, Dieckgraefe BK, Hruz PW, Rudnick DA. Delayed hepatocellular mitotic progression and impaired liver regeneration in early growth response-1-deficient mice. *J Biol Chem.* 2004;279:43107–16.
 11. Sha WC, Liou H-C, Tuomanen EI, Baltimore D. Targeted disruption of the p50 subunit of NF- κ B leads to multifocal defects in immune responses. *Cell.* 1995;80:321–30.
 12. Maeda S, Chang L, Li Z-W, Luo J-L, Leffert H, Karin M. IKK β is required for prevention of apoptosis mediated by cell-bound but not by circulating TNF α . *Immunit.* 2003;19:725–37.
 13. Shibata M, Lu T, Furuya T, Degtrev A, Mizushima N, Yoshimori T, et al. Regulation of intracellular accumulation of mutant huntingtin by beclin 1. *J Biol Chem.* 2006;281:14474–85.
 14. Pickford F, Masliah E, Britschgi M, Lucin K, Narasimhan R, Jaeger PA, et al. The autophagy-related protein beclin 1 shows reduced expression in early Alzheimer disease and regulates amyloid β accumulation in mice. *J Clin Invest.* 2008;118:2190–9.
 15. Pahl HL. Activators and target genes of Rel/NF-kappaB transcription factors. *Oncogene.* 1999a;18:6853–66.
 16. Pahl HL. Signal transduction from the endoplasmic reticulum to the cell nucleus. *Physiol Rev.* 1999b;79:683–701.
 17. Criollo A, Senovilla L, Authier H, Maiuri MC, Morselli E, Vitale I, et al. The IKK complex contributes to the induction of autophagy. *EMBO J.* 2010;29:619–31.
 18. Gohla A, Klement K, Piekorz RP, Pexa K, Vom Dahl S, Spicher K, Dreval V, Häussinger D, Birnbaumer L, Nürnberg B. An obligatory requirement for the heterotrimeric G protein Gi3 in the antiautophagic action of insulin in the liver. *Proc Natl Acad Sci USA.* 2011;104:3003–8.
 19. Xie S, Li J, Wang JH, Wu Q, Yang P, Hsu HC, Smythies LE, Mountz JD. IL-17 activates the canonical NF κ B signaling pathway in autoimmune B cells of BXD2 mice to upregulate the expression of regulators of G-protein signaling 16. *J Immunol.* 2010;184:2289–96.
 20. Zhong Z, Umemura A, Sanchez-Lopez E, Liang S, Shalpour S, Wong J, et al. NF κ B restricts inflammasome activation via elimination of damaged mitochondria. *Cell.* 2016;164:896–910.
 21. Carlson JA, Rogers BB, Sifers RN, Hawkins HK, Finegold MJ, Woo SL. Multiple tissues express alpha 1-antitrypsin in transgenic mice and man. *J Clin Invest.* 1988;5:26–36.
 22. Paranjpe S, Bowen WC, Bell AW, Nejak-Bowen K, Luo JH, Michalopoulos GK. Cell cycle effects resulting from inhibition of hepatocyte growth factor and its receptor c-Met in regenerating rat livers by RNA interference. *Hepatology.* 2007;45:1471–7.
 23. Osterreicher CH, Taura K, DeMinicis S, Seki E, Penz-Osterreicher M, Kodama Y, et al. Angiotensin-converting-enzyme 2 inhibits liver fibrosis in mice. *Hepatology.* 2009;50:929–38.
 24. Livak KJ, Schmittgen TD. Analysis of relative gene expression data using real-time quantitative PCR and the 2 $^{-\Delta\Delta CT}$ method. *Methods.* 2001;25:402–8.